Advances in Multiple Quantum Well IR Detectors

Prepared by

W. BLOSS, M. O'LOUGHLIN, and M. ROSENBLUTH
Electronics Technology Center
Technology Operations

30 October 1992

Prepared for

VICE PRESIDENT
Technology Operations

DTIC
ELECTE
FEB 0 8 1993
S E D

93-02278

Engineering and Technology Group

THE AEROSPACE CORPORATION
El Segundo, California

TECHNOLOGY OPERATIONS

The Aerospace Corporation functions as an "architect-engineer" for national security programs, specializing in advanced military space systems. The Corporation's Technology Operations supports the effective and timely development and operation of national security systems through scientific research and the application of advanced technology. Vital to the success of the Corporation is the technical staff's wide-ranging expertise and its ability to stay abreast of new technological developments and program support issues associated with rapidly evolving space systems. Contributing capabilities are provided by these individual Technology Centers:

Electronics Technology Center: Microelectronics, solid-state device physics, VLSI reliability, compound semiconductors, radiation hardening, data storage technologies, infrared detector devices and testing; electro-optics, quantum electronics, solid-state lasers, optical propagation and communications; cw and pulsed chemical laser development, optical resonators, beam control, atmospheric propagation, and laser effects and countermeasures; atomic frequency standards, applied laser spectroscopy, laser chemistry, laser optoelectronics, phase conjugation and coherent imaging, solar cell physics, battery electrochemistry, battery testing and evaluation.

Mechanics and Materials Technology Center: Evaluation and characterization of new materials: metals, alloys, ceramics, polymers and their composites, and new forms of carbon; development and analysis of thin films and deposition techniques; nondestructive evaluation, component failure analysis and reliability; fracture mechanics and stress corrosion; development and evaluation of hardened components; analysis and evaluation of materials at cryogenic and elevated temperatures; launch vehicle and reentry fluid mechanics, heat transfer and flight dynamics; chemical and electric propulsion; spacecraft structural mechanics, spacecraft survivability and vulnerability assessment; contamination, thermal and structural control; high temperature thermomechanics, gas kinetics and radiation; lubrication and surface phenomena.

Space and Environment Technology Center: Magnetospheric, auroral and cosmic ray physics, wave-particle interactions, magnetospheric plasma waves; atmospheric and ionospheric physics, density and composition of the upper atmosphere, remote sensing using atmospheric radiation; solar physics, infrared astronomy, infrared signature analysis; effects of solar activity, magnetic storms and nuclear explosions on the earth's atmosphere, ionosphere and magnetosphere; effects of electromagnetic and particulate radiations on space systems; space instrumentation; propellant chemistry, chemical dynamics, environmental chemistry, trace detection; atmospheric chemical reactions, atmospheric optics, light scattering, state-specific chemical reactions and radiative signatures of missile plumes, and sensor out-of-field-of-view rejection.

ADVANCES IN MULTIPLE QUANTUM WELL IR DETECTORS

Prepared by

W. Bloss, M. O'Loughlin, and M. Rosenbluth
Electronics Technology Center
Technology Operations

30 October 1992

Engineering and Technology Group
THE AEROSPACE CORPORATION
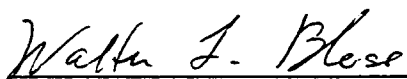El Segundo, CA 90245-4691

Prepared for

VICE PRESIDENT
Technology Operations

Accesion For		
NTIS CRA&I		☒
DTIC TAB		☐
Unannounced		☐
Justification		
By		
Distribution /		
Availability Codes		
Dist	Avail and / or Special	
A-1		

DTIC ⸺⸺⸺⸺⸺⸺D 1
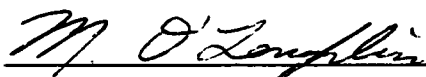
ADVANCES IN MULTIPLE QUANTUM WELL IR DETECTORS
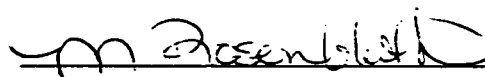
Prepared

W. Bloss

W. Bloss

M. O'loughlin

M. O'loughlin
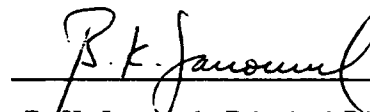
M. Rosenbluth

M. Rosenbluth

Approved

S. Feuerstein

S. Feuerstein, Acting Director
Solid State Electronics Department
Technology Operations

B. K. Janousek

B./K. Janousek, Principal Director
Electronics Technology Center
Technology Operations

NOTE

The material reproduced in this report originally appeared in the SPIE Proceedings *Infrared Sensors: Detectors, Electronics, and Signal Processing (1991)*. The ATR is published to document the work for the corporate record.

Advances in Multiple Quantum Well IR Detectors

Walter Bloss, Michael O'Loughlin, and Mary Rosenbluth

The Aerospace Corporation, P.O. Box 92957, Los Angeles, CA 90009

ABSTRACT

The performance of GaAs/AlGaAs multiple quantum well long-wavelength infrared detectors is evaluated for potential applications in focal plane arrays. A number of GaAs/AlGaAs quantum well infrared detectors with absorption between 7 to 12 μm have been fabricated and characterized. In these samples, the quantum well width and barrier height were held approximately constant, while the AlGaAs barrier thickness was varied from 300 to 500 Å. These detectors were characterized by FTIR absorption, dark current, responsivity, spectral noise density, and thermal activation energy measurements at temperatures ranging from 6 to 80 K. A maximum detectivity of 4×10^{13} cm√Hz/W at 6 K is obtained at $\lambda = 8.4$ μm for the 500 Å barrier sample.

1. INTRODUCTION

Photoconductors[1,2] fabricated from multiple, two-dimensional quantum wells of GaAs in an $Al_xGa_{1-x}As$ matrix represent a very promising approach to mid and long-wavelength infrared detection for a variety of applications. While performance requirements for any given application are unique, desirable attributes for any infrared detector are high detectivity, moderate operating temperature, and high producibility of large, highly uniform arrays. For instance, low background applications, such as satellite based astronomy or surveillance, require detectivities in excess of 10^{13} cm√Hz/W, with minimum operating temperatures fixed by the size/power of the cryocooler. For other applications, the size and uniformity of the imaging array are the driving consideration.[3] GaAs multiple quantum wells are grown by molecular beam epitaxy (MBE) or organometallic chemical vapor deposition (OMCVD) which are well-developed precision growth technologies allowing one to produce high quality structures with tailored band gap profiles and with layer thickness control on the atomic level. Device fabrication relies on standard processing techniques developed for digital and microwave GaAs integrated circuits which have been in use for many years and are relatively mature. Therefore, large uniform arrays can be produced at substantially reduced cost compared with competing technologies.

West and Eglash[4] were the first to demonstrate large intersubband absorption between confined states in quantum wells. In 1987, Levine and coworkers[5] fabricated the first quantum well (QW) IR detector operating at 10 μm. This detector design was based on a transition between two confined states in the quantum well and subsequent, tunneling out of the well by an applied electric field. Since this initial work, progress[6-10] in QW IR detectors has been quite rapid. In later work, thinner quantum wells were used pushing the excited state into the continuum enhancing detector performance. Detectors have been fabricated with detectivities of 1.0×10^{10} cm√Hz/W at a wavelength of 8.3 μm and temperature of 77 K.[11] Kinch and Yariv[12,13] presented an investigation of the fundamental physical limitations of individual QW IR detectors as compared to ideal HgCdTe detectors.

Levine, et. al.[14] have demonstrated a scanned 10-element linear GaAs quantum well array with a NEΔT of < 0.1° C. For a starring array, NEΔT of ~ 0.01° C are projected. Recently, a 128 x 128 GaAs QW IR focal plane array has been fabricated and has shown respectable performance, even in a geometry where the coupling to the photon is extremely small and hence, quantum efficiency is very low (~0.2 %).[15] Extremely low 1/f noise, low crosstalk (< 3 %), good uniformity, and a minimum resolvable temperature (MRT) of 0.03 K were measured. Although the aforementioned arrays are initial attempts to fabricate IR focal plane arrays, these results are very encouraging and demonstrate the potential of this technology. The above investigations focused on the 8-10 μm region, but more recent work has also demonstrated detectors with very respectable detectivities in the 3-5 μm region using InGaAs/InAlAs latticed matched to InP[16] which had a detectivity of 2.3×10^{10} cm√Hz/W at 120 K and using indirect AlGaAs barriers which had a detectivity of 1.1×10^{12} cm√Hz/W at 77 K operating in the photovoltaic mode.[17]

The primary focus of this work has been to characterize the effects of increased barrier thickness on detector dark current, responsivity, and detectivity. We have also investigated the low-temperature performance and the nature and origin of noise in such a detectors. Our demonstration of device detectivities in excess of 4 x 10^{13} cm√Hz/W at low temperatures provides evidence for the high-performance capabilities of this detector technology. In spite of these impressive recent developments, there are still several issues related to the optimum design of these detectors, quantum efficiency, and maximum coupling to the IR radiation.

2. MEASUREMENTS AND RESULTS

A series of QW IR detectors were designed and fabricated with AlGaAs barriers of increasing thickness, but other parameters remaining approximately constant, in order to maintain the same peak absorption from sample to sample. The detectors were designed to have a single bound state in the quantum well and the first excited state in the continuum above the AlGaAs conduction band edge. Figure 1 shows the device structure for a typical 10 μm quantum well detector. The difference in energy between the ground and continuum levels is fixed by the quantum well width and the aluminum mole fraction which determines the well depth. The epitaxial material used to fabricate the IR detectors was grown, under computer control, in a VG Semicon V80H Molecular Beam Epitaxy apparatus on a 50 mm diameter, undoped LEC, (100) GaAs wafer. The active structure of these samples consists of a 1 μm n-GaAs bottom contact layer, a 50 Å GaAs spacer layer, an IR active superlattice comprising 50 periods of $Al_{0.28}Ga_{0.72}As$ barriers with thicknesses L_b and 40 Å n-GaAs quantum wells followed by a 50 Å GaAs spacer layer, and finally a 0.5 or 1 μm n-GaAs top contact layer. A series of samples were grown with barrier thicknesses L_b of 300 Å, 400 Å, and 500 Å, and with the other growth parameters being maintained constant. The contact layers are doped with Si at a density 1 x 10^{18} cm^{-3} with the exception of the final 100 Å of each top contact which is doped to 4 x 10^{18} cm^{-3}. The center 50% of the quantum wells are doped with Si at a density of 2 x 10^{18} cm^{-3}, giving an average doping density in the wells of 1 x 10^{18} cm^{-3}. The approximate growth temperature was 620°C during deposition of the contact layers and 645°C during the superlattice growth.

Detectors were prepared using standard photolithographic techniques. The processing steps are outlined in figure 2. First the samples were etched through the superlattice and into the bottom contact layer to define circular mesas of various diameters. The top of each mesa and the bottom contact layer were then metallized with AuGe/Ni/Au. The ohmic contacts were alloyed at 425°C for 20 seconds in a rapid thermal anneal (RTA). The back of each sample was polished and coated with 3000 Å of Au for good IR reflectivity, and a 45° bevel was ground and polished on the edge of each sample as a means to introduce light with a component of the proper polarization for absorption by carriers in the quantum wells. Each sample was then mounted to a chip carrier on a 45° wedge such that the beveled edge of the sample was parallel to the surface of the carrier. The individual detectors were then wire bonded to the carrier leads.

The 45° bevel edge is a disadvantage of the GaAs QW IR detector. Selection rules dictate that only photons with a component of the electric field perpendicular to the superlattice layers can excite intersubband transitions within the QW. The standard geometry for focal plane arrays with light incident normal to the surface have zero absorption.[18] In a 45° bevel edge geometry, there is a finite component of the electric field along the superlattice axis; however, half the incident power is lost because of polarization (the parallel component) and another half is lost because of the angle of projection. Gratings can be applied to the surface to allow coupling to normal incidence light, and alleviate this problem to a certain degree.[18] Performance comparable to the 45° bevel edge coupler has been obtained with gratings, however, further improvement is possible.

The physical and optical properties of the epilayers were evaluated by Fourier transform infrared spectroscopy (FTIR), transmission electron microscopy (TEM), double crystal x-ray diffraction, and photoreflectance spectroscopy. Table 1 summarizes the results of these measurements on our samples. The samples are labeled and will be referred to in the text by their respective nominal barrier thicknesses, 300 Å-a. 300 Å-b, 400 Å, and 500 Å. The actual barrier thicknesses are slightly different from the nominal ones. The difference between samples a and b which both have a barrier thicknesses of 300 Å is the aluminum concentration. Sample b has a higher Al concentration and consequently, lower peak absorption wavelength (7.5 μm) since the absorption is set by the transition to the continuum (approximately the band edge of AlGaAs). The FTIR absorption spectra are obtained from waveguide samples prepared by polishing 45° facets on both ends of a 6 mm long strip of the epitaxial material. The absorption peaks of samples 300 Å-a, 400 Å, and 500 Å all occur close to 8.5 μm.

The dark current of each detector was measured with an HP 4145 parametric analyzer. A cold cap, maintained at 10 K, was used to shield the samples from background radiation. The temperature of the samples was measured with a Si diode placed in very close proximity. The measured dark current density at 6 K for samples with different barrier thicknesses as a function of voltage is shown in figure 3. There is a four order in magnitude drop in the dark current as the barrier thickness is increased from 300 to 500 Å. For a detector with a diameter of 100 μm, this corresponds to a dark current that is 7.85×10^{-5} times the current density, J. For voltages less than 4 V for the 500 Å sample and for 2 V for the 400 Å, the dark current is below the measurement floor of the parametric analyzer. To investigate the possibility of dark current resulting from leakage current along the side walls of the mesas, we compared the dark currents of a number of the 300 Å barrier detectors with diameters ranging from 50 to 250 μm, and found that the dark current scaled linearly with area for both samples. The dark current of the 300 Å barrier samples demonstrated the typical plateau region associated with high field domain formation between the ground state energy level in one well and the excited level in the continuum of the next.[19] The activation energy of the 300 Å-a and 300 Å-b barrier samples was determined from the Arrhenius plot of the dark current at 50 mV applied bias. At a temperature of approximately 65 K, the dominant current mechanism transitions from sequential resonant tunneling at lower temperatures to thermionic emission of carriers from the quantum wells at higher temperatures. The respective activation energies for thermionic emission were 0.135 eV and 0.151 eV. These values are calculated from the slope of the linear portion of the Arrhenius plot at high temperature. For both samples, the activation energy plus the Fermi energy is comparable to the measured peak responsivity energy.

The spectral noise density was measured using an HP 3582A spectrum analyzer. For all the detectors tested, the noise was spectrally flat over the range of the measurement, which was limited by 1/f noise at f<10 Hz and the RC roll-off at higher frequencies. Figure 4 shows the spectral noise density at 7 K for the 300 Å-a barrier sample as a function of the dark current. It is clear that the spectral noise density appears to be a fraction of the full shot noise, $\sqrt{(2qI)}$ for currents less than 10^{-7} A. At moderate biases, the spectral noise density to shot noise ratio is approximately 0.7 for all temperatures measured. The data at these biases can be explained using a model which takes into account the absorption coefficient (900 cm^{-1} as determined by FTIR), the photogenerated current gain as determined by the responsivity, the mean free path of the electrons, and the bias across the sample. Our model[9] predicts a spectral noise density/shot noise ratio of 0.6, in good agreement with the experimentally determined result. Recent results by Levine, et. al.[10] have shown that these detectors can have gains greater than one and act as standard photoconductors. We believe this to be true at high biases. In the high bias regime, the voltage drop across each barrier is ~120 meV which allows tunneling directly from the contact into the continuum. In this case, direct contact is made to the photoexcited carriers and a non-transit time limited lifetime with gain greater than unity is obtained. For biases lower than about 4 V (a dark current of 10^{-8} A corresponds to a 4 V applied bias in figure 4), our measured gain is less than one half, and the contacts may be playing a role in limiting the photocarrier lifetime.

To measure the responsivity, the samples were mounted in a liquid helium cooled dewar with a ZnSe, anti-reflection coated window. Infrared light from an external blackbody source was incident normal to the beveled edge of the sample and, after internal reflection from the back surface of the substrate, illuminated the detectors at a 45° angle to the superlattice. The infrared light was chopped, for background subtraction, and spectrally selected using a filter wheel with a range of 2.5-14.5 μm and a bandwidth of approximately 0.1 μm. To calculate the responsivity, the spectral power incident on the beveled edge of the sample was calculated from the temperature of the blackbody and its distance from the detector. The measured responsivity was corrected for the transmission coefficients of the ZnSe window and the filter wheel, as measured by FTIR, but not for reflection losses, polarization factors, or other parasitics inherent to this design. The accuracy of the responsivity measurements was verified with a calibrated Si:As detector.

The responsivity of detectors from the various samples is shown as a function of wavelength in figure 5. The responsivities peaked at approximately 8.2 μm, 7.7 μm, and 8.4 μm for the 300 Å-a, 400 Å, and 500 Å barrier samples, respectively. The peak responsivity for the samples was in the range of 0.3-0.5 A/W and increases slightly with temperature. A sample with twice the nominal dopant density is also presented in figure 5 and has about a 30 % higher responsivity. The wavelengths are somewhat shorter than that observed from the FTIR absorption measurements at room temperature. The discrepancy is explained by the increase in conduction band offset with decreasing temperature and also our observed shift in peak wavelength with applied bias at 6 K.

Using the measured responsivity (figure 5) and the spectral noise density, calculated from the measured dark current assuming full shot noise, we plot in figure 6 the detectivity of the 400 Å and 500 Å barrier samples as a

function of wavelength at 6 K. The assumption of full shot noise underestimates the detectivity since we typically find that the measured noise is less than the shot noise when it is large enough to be measured. The maximum detectivity measured for the 400 Å barrier sample was 3.0×10^{13} cm√Hz/W at 7.7 μm at 3 V applied bias. For the 500 Å barrier sample, the maximum detectivity was 4.2×10^{13} cm√Hz/W at 8.4 μm at 4 V applied bias. This increase in detectivity compared to our earlier 300 Å barrier results (10^{11} to 10^{12} cm√Hz/W) is a direct result of the decrease in tunneling dark current by increasing the barrier width. These curves do not necessarily represent the best performance because the optimum bias may be at a bias where we cannot measure the dark current. The 500 Å barrier sample shows a double peaked structure in the detectivity, arising from the structure in the responsivity. Note that the detectivity for the 500 Å barrier sample remains high at longer wavelengths. At 10 μm, the detectivity is still above 1×10^{13} cm√Hz/W.

In figures 7 and 8, we plot the measured detectivities as a function of temperature for the 300 Å-b and 400 Å barrier samples. The detectivity for the 300 Å-b barrier sample (figure 7) remains large (3×10^{12} cm√Hz/W) until 50 K where it begins to steadily decrease. The detectivity of the 400 Å sample (figure 8) is quite high at very low temperatures and is still ~ 10^{13} cm√Hz/W at T ~ 25 K at a bias of 3 V. At temperatures greater than 25 K, the detectivity decreases rapidly due to the increase in the thermionic component of the dark current. Although the dark current was immeasurable at T < 25 K and 1 V bias, we can extrapolate that the detectivity at those temperatures is in excess of 3×10^{13} cm√Hz/W.

3. CONCLUSION

In this work, we have investigated the performance of QW IR detectors as a function of increasing barrier thickness. Thick barriers (~500 Å) significantly reduce the tunneling dark current at low temperatures resulting in high detectivites. However, at high temperatures, the dark current is dominated by thermionic emission. In order for these detectors to operate with high detectivities at higher temperatures, methods must be developed to inhibit thermionic emission.

The real advantage of GaAs QW detectors over competing technologies is in its ease of manufacturability and reproducibility. Large arrays can be made at substantially reduced cost and with high uniformity of elements in the array. While this technology is already compatible with GaAs microelectronics, these detectors can also be grown on Si substrates allowing thermal match to silicon read-out electronics. Also, the MBE growth process allows precise control of the band profiles permitting device optimization and tunability. By growing these QW structures one on top of another, compact multicolor arrays can be made. Although these multiquantum well infrared detectors may not represent the pinnacle of performance in any of the individual desirable detector attributes, they are competitive with and perhaps superior to other technologies when all attributes are considered together.

4. ACKNOWLEDGEMENTS

5. REFERENCES

1. J. C. Smith, L. C. Chui, S. Margalit, A. Yariv, and A. Y. Cho, "A new infrared detector using electron emission from multiple quantum wells," J. Vac. Sci. Technol. B 1, (1983).
2. D. D. Coon and R. P. G. Karunasiri, "New mode of IR detection using quantum wells," Appl. Phys. Lett. 45, 649 (1984).
3. B. F. Levine, G. Hasnain, C. G. Bethea, and N. Chand, "Broadband 8-12 μm high-sensitivity GaAs quantum well infrared photodetector," Appl. Phys. Lett. 54, 2704 (1989).
4. L. C. West and S. J. Eglash, "First observation of an extremely large dipole infrared transiton within the conduction band of a GaAs quantum well," Appl. Phys. Lett. 46, 1156 (1985).
5. B. F. Levine, K. K. Choi, C. G. Bethea, J. Walker, and R. J. Malik, "New 10 μm infrared detector using intersubband absorption in resonant tunneling GaAlAs superlattice," Appl. Phys. Lett. 50, 1092 (1987).

6. K. K. Choi, B. F. Levine, C. G. Bethea, J. Walker, and R. J. Malik, "Multiple quantum well 10 μm GaAs/Al$_x$Ga$_{1-x}$As infrared detector with improved responsivity," Appl. Phys. Lett. 50, 1814 (1987).

7. B. F. Levine, C. G. Bethea, K. K. Choi, J. Walker, and R. J. Malik, "Bound-to-extended state absorption GaAs superlattice transport infrared detectors," J. Appl. Phys. 64, 1591 (1988).

8. B. F. Levine, C. G. Bethea, G. Hasnain, V. O. Shen, E. Pelve, R. R. Abbot, and S. J. Hsieh, "High sensitivity low dark current 10 μm GaAs quantum well infrared photodetectors," Appl. Phys. Lett. 56, 851 (1990).

9. B. K. Janousek, M. J. Daugherty, W. L. Bloss, M. L. Rosenbluth, M. J. O'Loughlin, H. Kanter, F. J. DeLuccia, and L. E. Perry, "High detectivity GaAs quantum well infrared detectors with peak responsivity at 8.2 μm", J. Appl. Phys. 67, 7608 (1990).

10. G. Hasnain, B. F. Levine, S. Gunapala, and Naresh Chand, "Large photoconductive gain in quantum well infrared photodetectors," Appl. Phys. Lett. 57, 608 (1990).

11. B. F. Levine, C. G. Bethea, G. Hasnain, J. Walker, and R. J. Malik, "High detectivity D*=1.0 x10^{10} cm$\sqrt{}$Hz/W GaAs/AlGaAs multiquantum well λ=8.3 μm infrared detector," Appl. Phys. Lett. 53, 296 (1988).

12. M. A. Kinch and A. Yariv, "Performance limitations of GaAs/AlGaAs infrared superlattices," Appl. Phys. Lett. 55, 2093 (1989).

13. B. F. Levine, Comment on "Performance limitations of GaAs/AlGaAs infrared superlattices," Appl. Phys. Lett. 56, 2354 (1990).

14. C. G. Bethea, B. F. Levine, V. O. Shen, R. R. Abbott, and S. J. Hseih, "10-μm GaAs/AlGaAs multiquantun well scanned array infrared imaging camera," IEEE Trans. Electron Dev. 38, 1118 (1991).

15. L. J. Kozlowski, G. M. Williams, G. J. Sullivan, C. W. Farley, R. J. Anderson, J. Chen, D. T. Cheung, W. E. Tennant, and R. E. DeWames, "LWIR 128 x 128 GaAs/AlGaAs multiple quantum well hybrid focal plane array, IEEE Trans. Electron Dev. 38, 1124 (1991).

16. G. Hasnain, B. F. Levine, D. L. Sivco, and A. Y. Cho, "Mid-infrared detectors in the 3-5 μm band using bound to continuum state absorption in InGaAs/InAlAs multiquantum well structures," Appl. Phys. Lett. 56, 770 (1990).

17. B. F. Levine, S. D. Gunapala, and R. F. Kopf, "Photovoltaic GaAs quantum well infrared detectors at 4.2 μm using indirect Al$_x$Ga$_{1-x}$As barriers," Appl. Phys. Lett. 58, 1551 (1991).

18. G. Hasnain, B. F. Levine, C. G. Bethea, R. A. Logan, J. Walker, and R. J. Malik, " GaAs/AlGaAs multiquantum well infrared detector arrays using etched grating," Appl. Phys. Lett. 54, 2515 (1989).

19. K. K. Choi, B. F. Levine, R. J. Malik, J. Walker, and C. G. Bethea, "Periodic negative conductance by sequential resonant tunneling through an expanding high-field superlattice domain," Phys. Rev. B 35, 4172 (1987).

Table 1

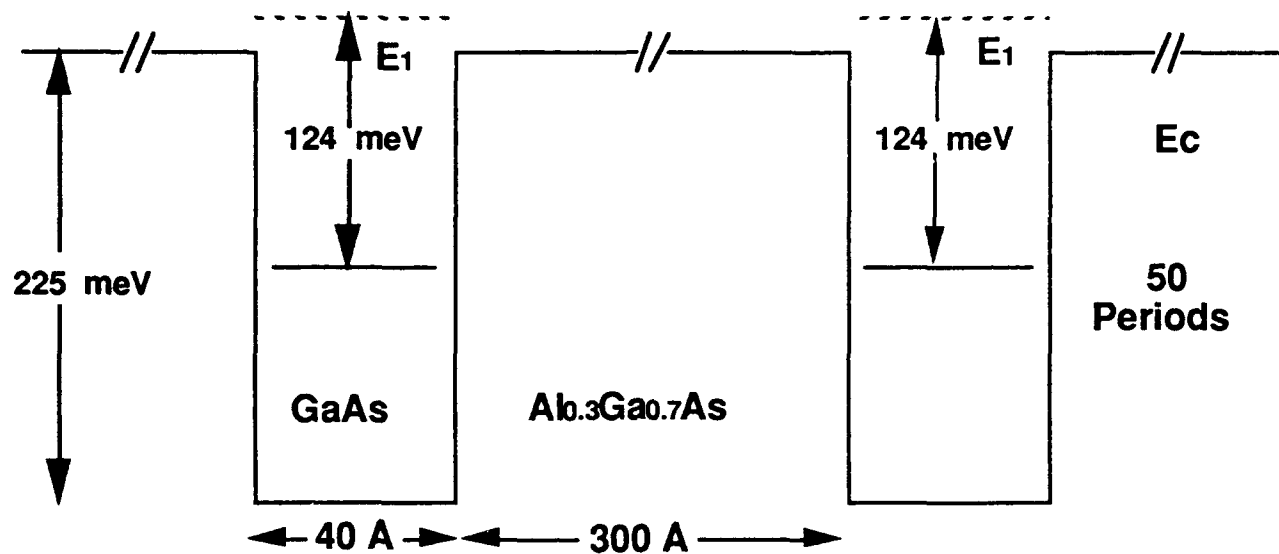| Sample	300 Å-a	300 Å-b	400 Å	500 Å
Peak Wavelength (FTIR)	8.9 μm	7.5 μm	8.3 μm	8.5 μm
Superlattice Period (x-ray)		346 Å	528 Å	432 Å
Superlattice Period (TEM)	320 Å			
Al Mole Fraction (x-ray)		0.35	0.31	0.31
Al Mole Fraction (modulation spectroscopy)	0.29	0.33		

Fig. 1. Typical multiple quantum well structure designed for 10 μm detection.
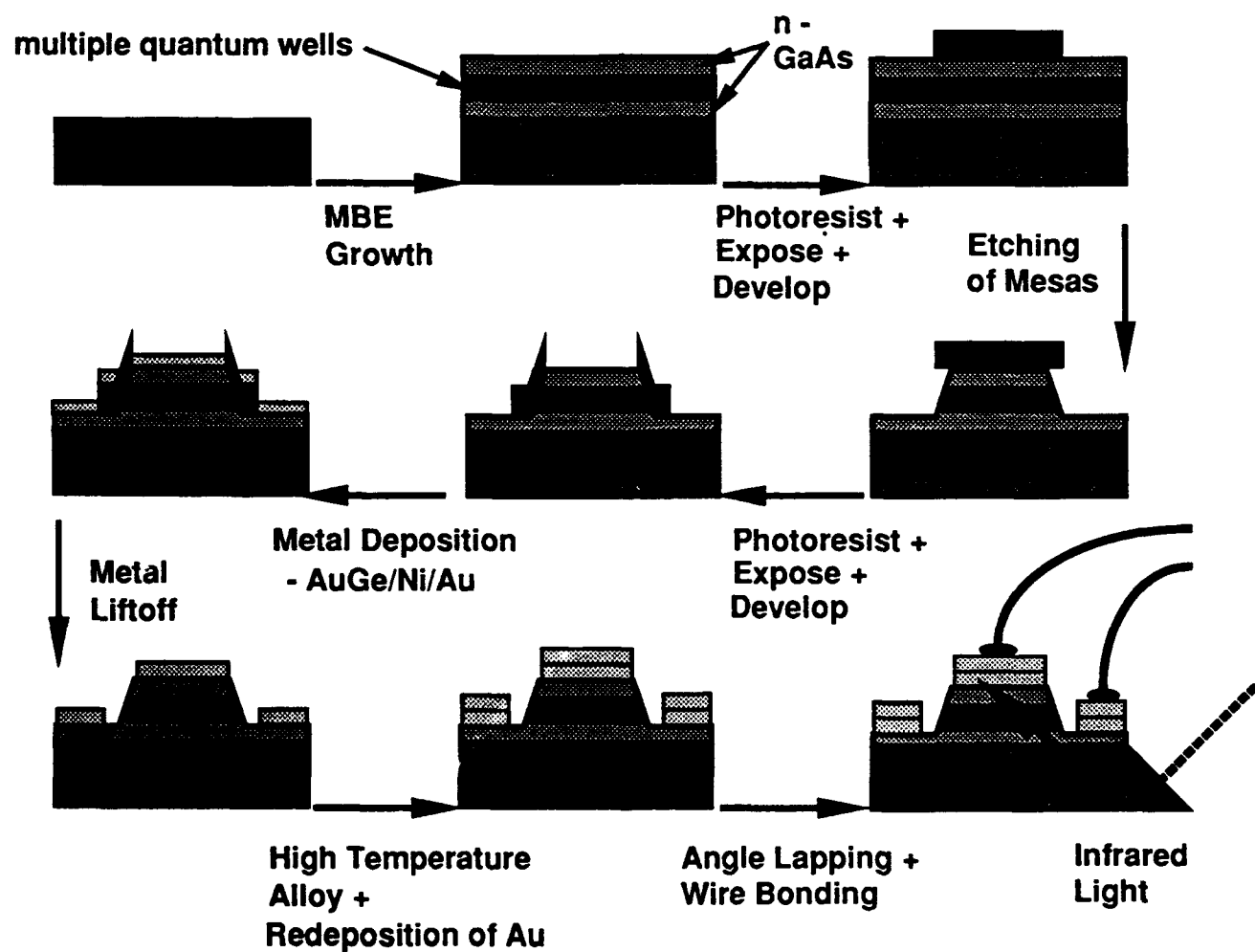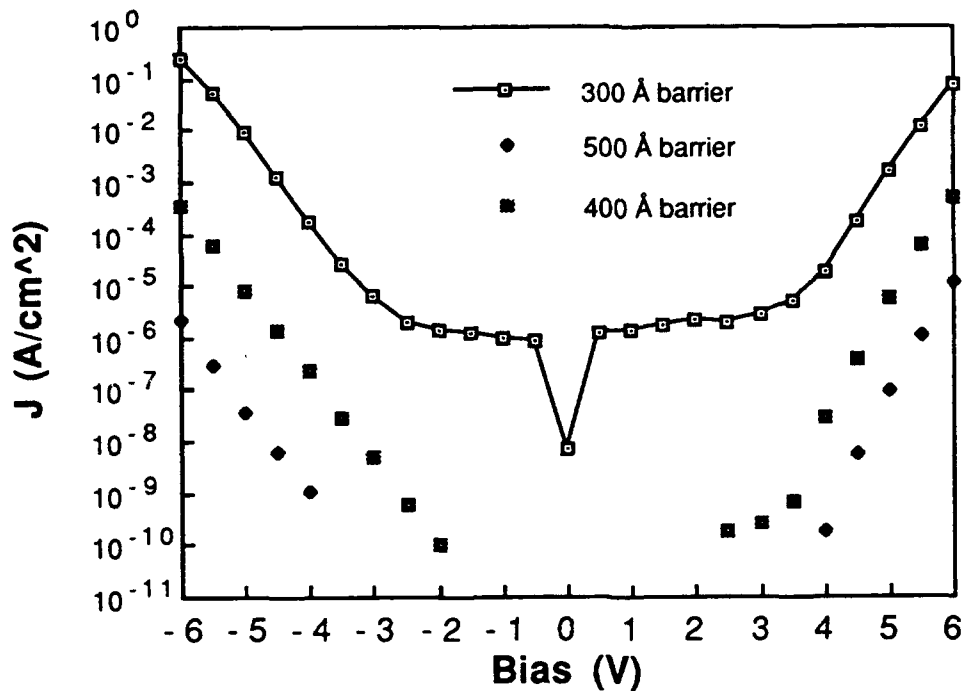

Fig. 2. IR detector processing flow chart.

Fig. 3. Detector dark current density for different barrier thicknesses as a function of bias at 6 K.
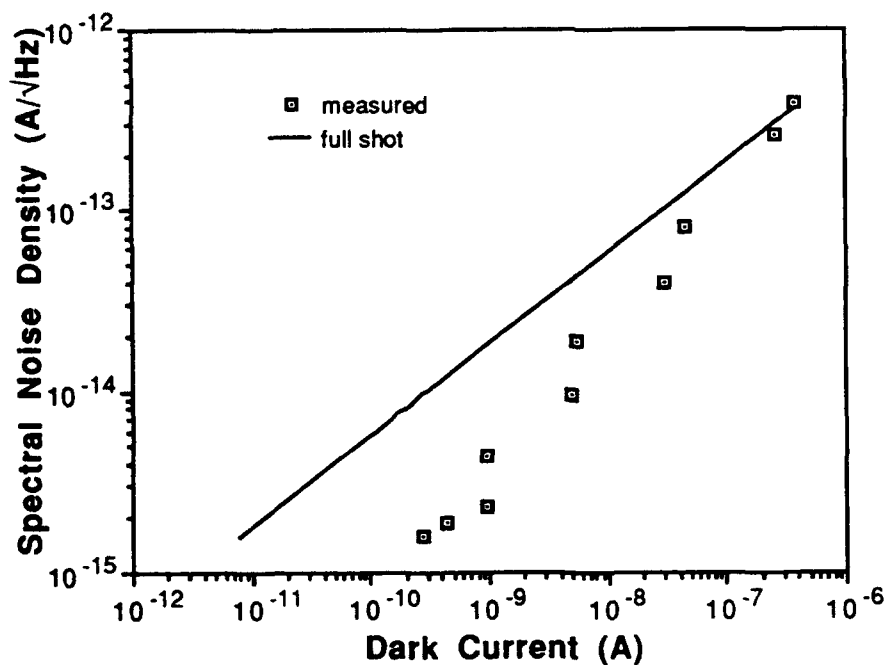

Fig. 4. Measured noise performance as a function of applied bias for the 300 Å-a barrier sample. The dots are the experimental data points and the solid line is the full shot noise derived from the dark current.
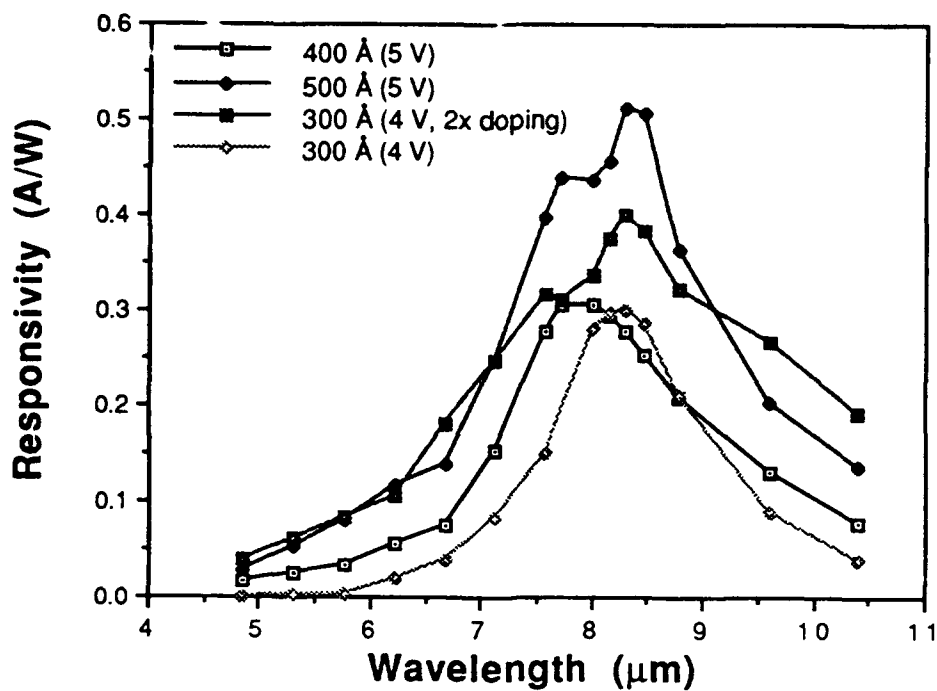
Fig. 5. Responsivity as a function of wavelength for samples with different barrier widths and dopant density.
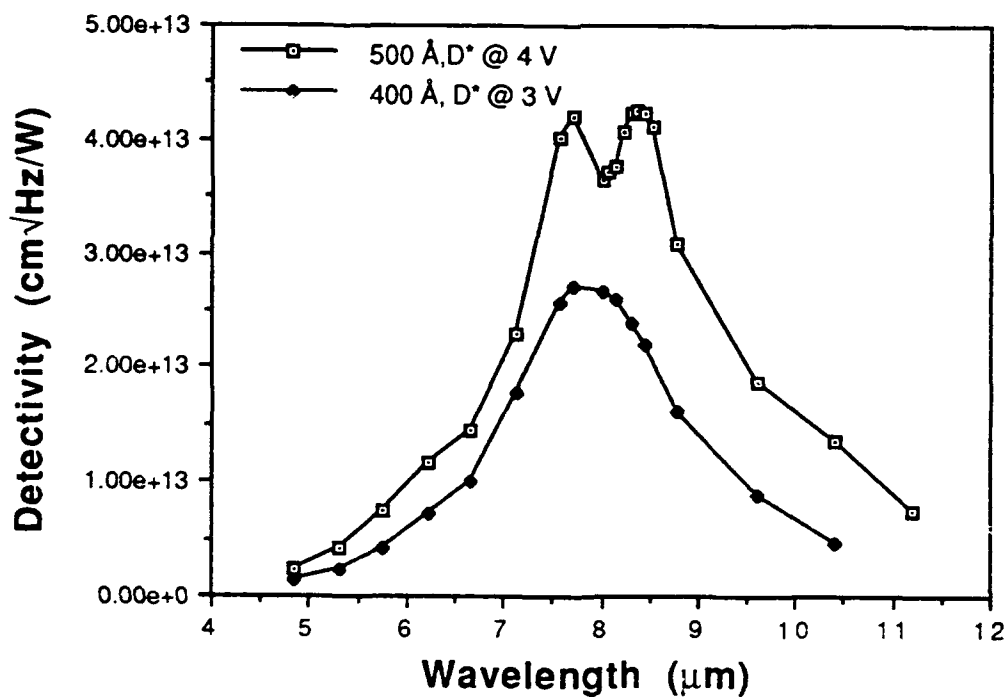

Fig. 6. Detectivity, calculated assuming full shot noise, as a function of wavelength for the 400 Å and 500 Å barrier samples.
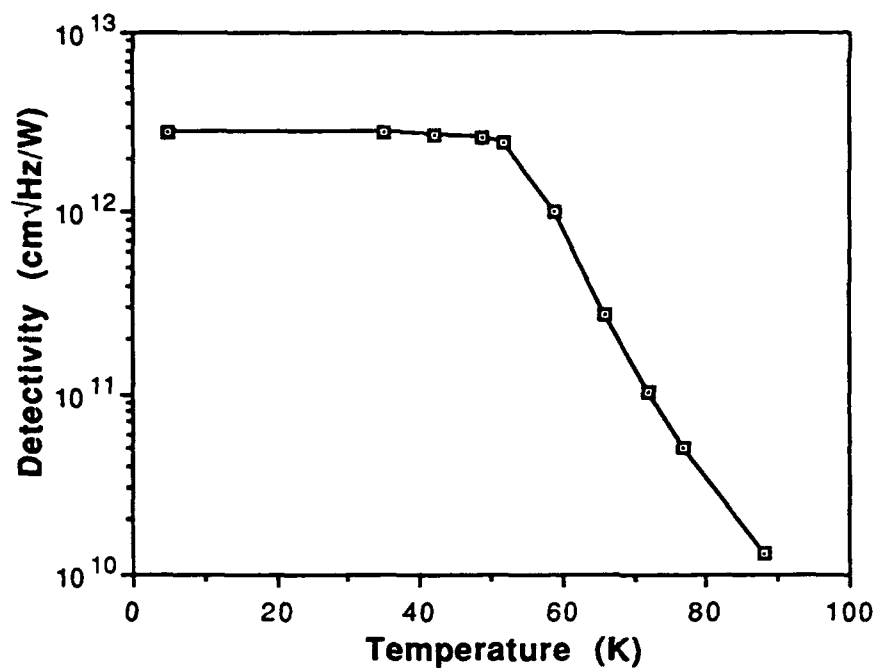
Fig. 7. Detectivity of the 300 Å-b barrier sample at 7.6 μm as a function of temperature At each temperature the bias is optimized for maximum D*.
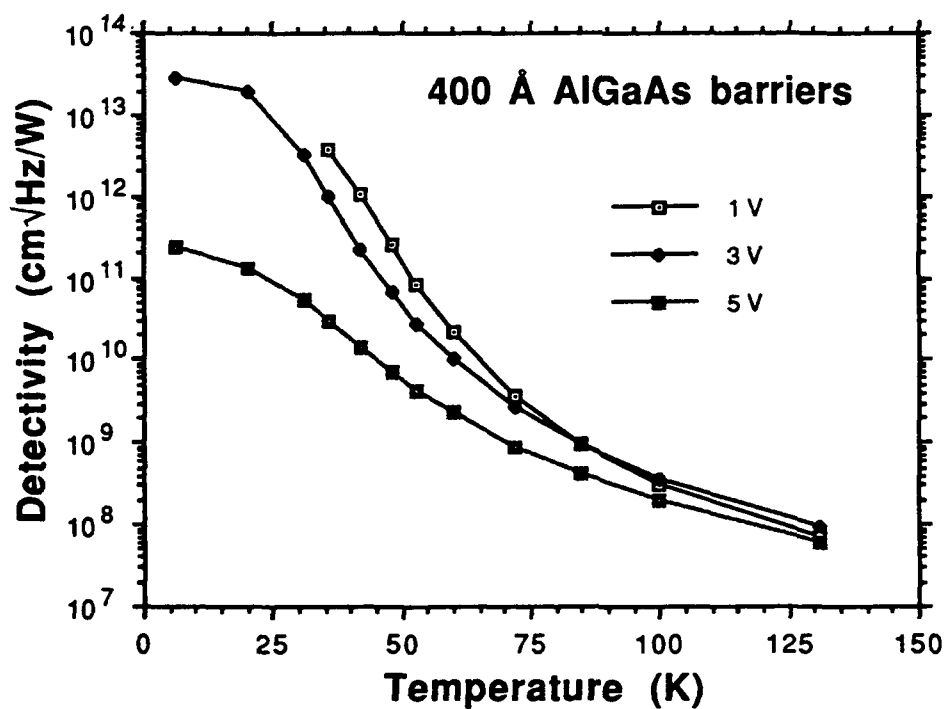

Fig. 8. Detectivity of the 400 Å barrier sample as a function of temperature and bias.